



3D brain image-based Alzheimer's disease detection techniques using fish swarm optimizer's deep convolution Siamese neural network

Rajaram Sampath^{1,2}  | Manickam Baskar¹ 

¹Department of Computing Technologies, School of Computing, College of Engineering and Technology, SRM Institute of Science and Technology, Chengalpattu, Tamilnadu, India

²Associate Professor, Dhaanish Ahmed College of Engineering, Chennai, Tamilnadu, India

Correspondence

Manickam Baskar, Associate Professor, Department of Computing Technologies, School of Computing, College of Engineering and Technology, SRM Institute of Science and Technology, Kattankulathur, Chengalpattu, Tamilnadu, India-603 203
Email: baashkarcse@gmail.com

Abstract

Alzheimer's disease (AD), a chronic syndrome that impacts the brain, is the most prevalent form of dementia. Dementia is a brain disease that severely affects an individual's ability to perform daily activities. It starts slowly affects the brain and creates a loss of memory, language, problem-solving and other thinking abilities. Hence, early detection is essential to avoid the severity of this illness. Neuroimaging techniques are widely recommended diagnosing approaches by medicos for early AD detection. However, detecting AD using imaging is a challenging and time-consuming task for human expertise. Many machine learning techniques already exist in automatic AD stages detection, but these techniques are failed to handle main issues in AD detection systems such, as preserving and identifying precise biomarker regions certainty handling and; in this research, a new convolution-based AD stages detection framework is introduced to resolve the earlier detection system's challenges and issues. The first two convolution layers contain resizing, adaptive filtering, and adaptive histogram equalization techniques to enhance the image quality, preserving biomarker features. The third layer contains the Voxel-based Morphometry (VBM) technique to segment the exact biomarker regions of AD stages from brain MRI images. The segmented biomarker feature is extracted and selected in the fourth and fifth layers to identify exact significant biomarker features to reduce the overfitting problem during the model training. Finally, the new food source direction investigation feature of the fish swarm optimizer (FSO) is incorporated in the deep Siamese neural network (DSNN) classification phase, which reduces the uncertainty issue during model training. The efficiency is evaluated using ADNI, AIBL, and OASIS database MRI images with various accuracy metrics. The evolution results show that the new framework is obtained a higher accuracy rate of 99.89% in AD stages detection than the comparison classifiers.

KEYWORDS

3D MRI brain image, Alzheimer's disease, biomarker features, deep convolution Siamese neural network, feature extraction, fish swarm optimizer, image enhancement, segmentation

1 | INTRODUCTION

AD is a permanent progressive neurodegenerative disorder (Ebrahimi-Ghahnavieh et al., 2020) and the most widespread type of dementia, containing an anticipated 60%–80% of all dementia cases. It usually starts in middle or old age, probably initiated by abnormal protein growth in and around the neuron. It leads to a steady weakening in memory. Clinical stages (Kazemi & Houghten, 2018) of AD are cognitive normal (CN), Mild cognitive impairment MCI, significant memory concern (SMC), and Alzheimer's disease (AD) (Solano-Rojas et al., 2020). The patient with the CN stage of AD generally does not have any AD symptoms such as depression, MCI or dementia. SMC is self-reporting considerable memory apprehension from the patient, measured by the cognitive variation index and clinical dementia rating of 0. At this stage, patients score within the normal range of cognition. MCI patients have reported subjective memory concern either alone or clinician; it is classified as early and later stages MCI. AD's final stage is a progressive disease, where dementia signs slowly worsen over a few years. Present medication cannot stop the disease from developing; however, it can provisionally slow the worsening of dementia signs and enhance life quality for those with AD. Therefore, early detection of all the AD stages (Ju et al., 2019) is essential to control the development of MCI to AD (Beheshti et al., 2017). The diagnosis is based on clinical examination and comprehensive interviews of the patient and their relatives, and these approaches are difficult and time-consuming tasks. Therefore, AD is currently diagnosed by Neuroimaging (Shi et al., 2017), cognitive tests and Cerebrospinal Fluid Analysis CFA. Brain Neuroimaging techniques are widely recommended diagnosing approaches by medicos for early AD detection (Chen et al., 2018). There are three subsets of Alzheimer's disease based on the distribution of tau-related pathology and regional brain atrophy: normal, limbic-predominant, and hippocampal-sparing. Some of the neuroimaging techniques (Lu et al., 2018) for examining AD are X-ray, computerized tomography (CT) scan and positron emission tomography (PET) and MRI (Faturrahman et al., 2017). The brain 3D MRI (Mori et al., 2016) technology can deliver clear images of parts of the brain that can be seen with an X-ray, CT scan, making it predominantly valuable for diagnosing the pituitary gland and brain stem. Therefore, 3D MRI images are taken for the learning and prediction of AD's biomarkers features. Strong learning algorithms must process and detect the AD disease stages (Nawaz et al., 2020) using 3D MRI brain images for high throughput. There are lots of machine learning algorithms (Aderghal et al., 2018; Cheng & Liu, 2017; Dolph et al., 2017; Jha & Kwon, 2017) that already exist in early AD stages detection approaches. Most of the existing AD detection techniques (Gupta et al., 2019; Kumari et al., 2020) failed to handle main issues in detection systems such as preserving biomarker region identification, uncertainty handling and overfitting avoidance. In this research, the following techniques are incorporated in the detection system to achieve the challenges; rescaling, adaptive filtering, and adaptive histogram equalization techniques have been incorporated to enhance the input image quality and preserve biomarker features. The VBM technique focuses on segmenting the exact biomarker regions of AD from the MRI image. The biomarker feature extraction and selection techniques help identify the significant biomarker features, reducing the overfitting problem during the model training. The fish's new direction following the function-based food investigation feature of the FSO is incorporated in the DSNN model helps reduce the uncertainty issue. Hence, the new classifier efficiently predicts uncertain brain MRI images during the testing process. The new classification approach's efficiency is compared with various existing deep learning-based classification approaches discussed in a related study. To enhance the quality of the input image and preserve biomarker features, this research used rescaling, adaptive filtering, and adaptive histogram equalization techniques in the detection system. The VBM technique aims to identify the specific biomarker regions associated with Alzheimer's disease from an MRI image.

The research's organization work is explained in the subsequent order; Section 1 describes the introduction of AD disease and diagnosing techniques and problem definition. Section 2 describes the recent research and methodologies utilized for the AD detection system. Section 3 discusses image database information and the methodologies used in this research. Section 4 describes the evaluation results of the classification approach and discussion. Finally, Section 5 describes these research findings and feature the research conclusion. The classification model's detailed descriptions and evaluation performance are explained in the subsequent sections. The consequent section describes the literature review in detail.

As many machine learning techniques exist for AD stages detection, whereas these techniques fail to address some of the most important issues in AD detection systems, such as preserving and identifying precise biomarker regions certainty handling and; in this research, an AD stages detection framework based on convolutional neural networks is introduced to resolve the earlier detection system's challenges and issues, as well.

2 | LITERATURE REVIEW

Several studies have been investigated neuroimaging based on the early stages of AD detection. This section discusses the various related studies of MRI image processing methodologies and various researches on AD detection. This research (Gupta & Verma, 2020) designed an extension of the 1-D adaptive filter in 2D form and a new 2D adaptive filter. The performance evolution result shows that the new adaptive filter achieves superior performance than other comparison filtering approaches, and it is useful for the reconstruction of the biomedical image. This study (Singh et al., 2020) introduces a novel framework for robust contrast enhancement and multiplicative noise suppression and demonstrates its efficiency utilizing an extensive range of clinical ultrasound scans. This framework's feature enhancement phase utilizes an enhanced CLAHE

technique for improving the texture and contrast of the ultrasound video. This research (Spalthoff et al., 2018) shows that the various facets of morphology can be divided into a meaningful full manner and how the various morphometric constraints can be utilized to distinguish effects. It helps in the identification of marker relevance. The (Damodaran et al., 2017) study established a new feature selection approach for hyperspectral image classification. The 'new class separability measure' based on Surrogate Kernal and Hilbert Schmidt independence criteria (HSIC) has been supported by empirical kernel maps in the RKHS. In the research (Garg & Dhiman, 2020), feature extraction and reduction are incorporated in content-based image retrieval techniques. The approach contains complete structural feature extraction and the grey level co-occurrence matrix (GLCM) descriptor to extract the image's texture's statistical features. The GLCM based feature extraction techniques help classify the CORAL dataset information with maximum accuracy. The research (Lucas et al., 2020) is developed a wavelet, transform-based feature extraction technique, which is combined with an evolving neural network to detect and locate high impedance faults in a time-varying distributed generation system. This approach gives promising results in terms of accuracy and robustness. In this research (Al-Kadi, 2017), the Gabor filter energy has used each magnitude response's output, combined with four other fixed resolution texture signatures with and without cell nuclei segmentation. The maximum accuracy rate has been obtained during the evaluation when combining the Gabor filter energy and meningioma sub-image fractal signature. In this research (Ye et al., 2018), an improved artificial fish swarm optimizer is introduced for weapon target assignment problems in the air defence system to improve the assignment rate. The individual visual of artificial fish and genetic operator in PSO are incorporated to avoid local extremum traps. The above-discussed methodologies' collective features are taken to develop a convolution layer to the AD detection framework. In this research (Liu et al., 2019), a deep learning model exploiting the Siamese neural network learned on paired lateral inter-hemispheric areas is utilized to control and differentiate the power of entire brain volumetric irregularity. The approach utilizes the MRI Cloud pipeline to provide low-dimensional volumetric features of pre-defined atlas brain structures and a novel non-linear kernel trick to standardize these features to condense batch possessions across datasets and populations. The DSNN perform well on some metrics by clearly encoding the irregularity in brain volume.

Above Table 1 shows the recent related study on AD stages detection approaches. It contains a reference, Database, samples counts of AD stages, imaging/input types, the research contribution, and efficiency obtained by the methodologies. Most of the research papers discussed in this section Utilized CNN and its categories of models for detecting various AD stages. Few authors are investigated learning concepts by using CNN models to improve prediction accuracy. These CNN classifiers perform well, especially on image datasets. All the AD classification models discussed in this section perform poorly with uncertain images samples. Very little research included preprocessing phases like rescaling and enhancement. The framework for image enhancement has used sliding window adaptive histogram equalization approaches. For the first time, this method of MRI image equalization does not use just one histogram to redistribute the image's lightness value. Therefore, the edge of the brain MRI image slices is enhanced, making it ideal for local contrast. Most of the approaches are failed to focus on exact biomarker regions and their feature information. The early CNN model has overfitting issues because of too much image feature information. According to early studies, none of the research work addresses these issues. Therefore, a strong classification model has been required to detect the various AD stages without the issues mentioned above. In this research, the following methodologies are incorporated into the classification framework to resolve the gaps' research. The rescaling, adaptive filtering, and adaptive histogram equalization techniques have been incorporated to enhance image quality, reduce the automation system's storage capacity, and preserve biomarker features. The VBM technique segments the exact biomarker regions of Alzheimer's disease from the MRI image. Utilizing the biomarker feature extraction and irrelevant feature information reduction techniques utilization help identify the significant biomarker features, reducing the overfitting problem during the model training. The fish swarm optimiser's following behaviour in the DSNN network helps optimize the uncertainty issues.

2.1 | Objectives

This research's main objective is to reduce the uncertainty and overfitting issues, focusing on biomarker region preserving and identification issues to train the biomarker information of AD stages. The research objective fulfils the research gaps and improves the classification model's performance in AD stages detection. The classification model's performance has been compared with existing traditional and recent CNN models, and the efficiency is tested with various accuracy metrics. The subsequent section discusses the methodologies utilized to process the image for detecting AD stages.

3 | METHODOLOGIES OF FSODSNN BASED AD STAGES DETECTION

Figure 1 illustrates the AD detection process; According to the AD detection system, initially, the 3D MRI brain image had been collected from patients in scan centres. The MRI scan image has been taken as input to the detection system. In the second stage, all the input MRI images are resized in common size. In the first two convolution layers, filtering and image enchantment techniques have been applied to improve the image's quality. The third convolution layer is responsible for VBM based biomarker region extraction from the enhanced image. The fourth convolution

TABLE 1 Related study on AD stages detection

Reference	Dataset name	Sample size	Image type	Methodologies	Accuracy	Contribution
(Liu et al., 2019)	ADNI, BIO CARD	3566 744	MRI 1.5T T1	Deep Siamese neural network	99.86% (Sensitivity)	A novel non-linear kernel trick is used to standardize the extracted features
(Beheshti et al., 2017)	ADNI	458	3D T1 weighted MRI	SVM	93.01%	Fisher criteria used in genetic algorithm for feature selection
(Ullah et al., 2018)	OASIS	416	3D MRI	Deep convolutional neural network (CNN)	80%	Utilized Deep CNN
(Ebrahimi-Ghahnavieh et al., 2019)	ADNI	177 (48 axial, 72 coronal, 57 sagittal)	3D MRI - 2D slices	2D CNN (GoogleNet, AlexNet, VGG Net-16&19, SqueezeNet, ResNet 18, 50&101, Inceptionv3) + Long Short Term Memory (LSTM)	90.62%	Applied Transfer learning (CNN trained LSTM)
(Karasawa et al., 2018)	ADNI	1728 (574 NC, 450 MCI, 358 late MCI, 366 AD)	MRI	3DCNNResNet	94% (Accuracy)	39 layered 3D CNNResnet
(Spasov et al., 2018)	ADNI	200 (normal), 400 MCI, 200 AD	MRI	CNN	99%	Designed a CNN model to learn three types of input (MRI, clinical assessment and genetic [APOe4] measures) to reduce overfitting
(Liu et al., 2020)	ADNI	97 AD, 233 MCI, 119 NC	T1 MRI	Multi-task deep CNN+ 3D DenseNet	88.9%, 92.5% (ROC)	Multi-model deep learning framework for hippocampal segmentation and classification. (AUC -Area Under ROC Curve)
(Lee et al., 2019)	ADNI	1618 (415 CN, 865 MCI and 338 AD)	MRI + Longitudinal cerebrospinal fluid (CSF)	GRU	81%	Multi-model deep learning framework, which Integrating multi-domain data
(Hon & Khan, 2017)	OASIS	6400	MRI	Inception V4 + VGG16	96.25%	Transfer learning
(Wang et al., 2018)	A local hospital, OASIS	98 AD, 98 HC	3.0 T MRI	8 layered CNN	97.65%	CNN with Leaky Rectified Linear Unit and Max Poling
(Allioui et al., 2020)	OASIS	609 NC, 489 AD	MRI	PSO + CNN	94.73%	Utilization of PSO in CNN to minimize training loss
(Acharya et al., 2019)	University of Malaya Medical Center	55 AD 110 NC	T2 MRI	Shearlet Transform (ST) + KNN	98.48%	Shearlet Transform based feature extraction techniques
(Fan et al., 2020)	ADNI	688	MRI	SVM	97.87%	Utilized SVM classifier to examine the AD detection performance
(Li et al., 2020)	ADNI	877 MCI+c, 1680 MCI-nc	MRI views: (H), (EC), (MTC), (FG), and(WB)	Principal component analysis through conditional exception (PCAE)	80% (AUC)	Developed ROI based longitudinal data prediction framework. Hippocampus (H), entorhinal cortex (EC), middle temporal cortex (MTC), Fusiform gyrus (FG), and whole-brain (WB)

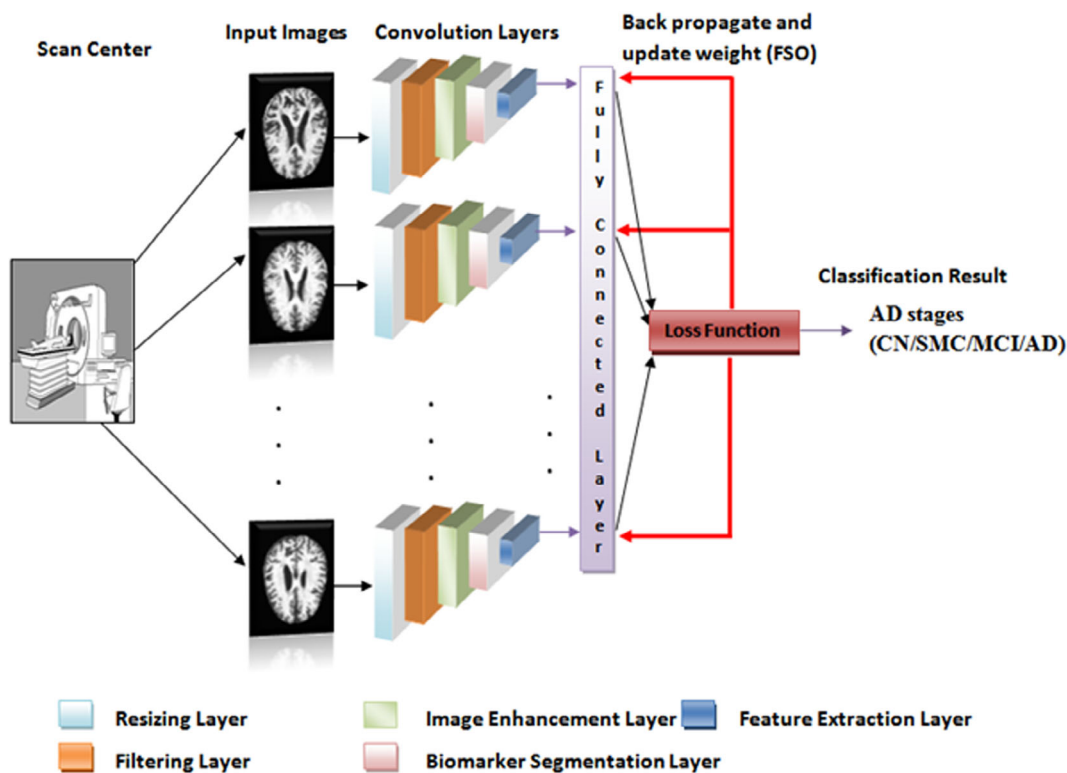


FIGURE 1 General structure of FSODSNN based AD stages detection

performs the process of the biomarker features, and the fifth convolution layer is responsible for the significant selection of biomarkers. The consolidated convolution features (constructed feature vector) in deep, fully connected utilized to train the DSNN model during the model training. Next, calculate the loss and backpropagate the network based on the loss value and update the weight using FSO. Finally, biomarker features are trained to create patterns and generate prediction reports (detect AD stages).

3.1 | 3D MRI data acquisition

Generally, the input image has been collected from the 3 Tesla T1 weighted imaged MRI scanner. However, in this research, the 3D MRI (Wee et al., 2019) baseline images are taken from the Alzheimer's Disease Neuroimaging Initiative (ADNI) database, obtained from 3 Tesla T1 weighted images. The structural T1 weighted MRI scan is obtained utilizing 1.5 T or 3 T scanners. The typical 1.5 T attainment variables repetition time (RT) = 2400 ms, minimum full echo time (ET), inversion time (IT) = 1000 ms, flip angle = 8° , field of view (FOV) = $240 \times 240 \text{ mm}^2$, acquisition matrix = $256 \times 256 \times 170$ in x, y, and z dimensions. Capturing a voxel size of $1.25 \times 1.25 \times 1.2 \text{ mm}^3$. The acquisition parameter value of 3 T scans are RT = 2300 mm, minimum full of ET, IT = 900 ms, flip angle = 8° , FOV = $260 \times 260 \text{ mm}^2$, acquisition matrix = $256 \times 256 \times 170$, Capturing a voxel size of $1.0 \times 1.0 \times 1.2 \text{ mm}^3$. The DSNN model is trained using the consolidated convolution features (built feature vector) deep, completely connected. Backpropagation and weight updates are done using FSO, which estimates loss and backpropagates the network. In the end, biomarker characteristics are taught to establish patterns and generate forecast reports (detect AD stages).

The overall AD dataset is separated into two sets as test and training; it contains four different classes such as non Demented/CN, very mild Demented/SMC, mild Demented/MCI and Moderated/AD. These MRI images are collected from various databases, discussed later in this section.

Table 2 contains overall images collected from the various data sources like ADNI, AIBL and OASIS. Alzheimer's Disease Neuroimaging Initiative (ADNI) database (ADNI, n.d.) is categorized into four types of datasets ADNI-1, ADNI-GO(Grand Opportunities), ADNI-2, ADNI-3. The ADNI-1 & ADNI-GO jointly contains 400 SMC, 400 MCI, 200 AD. The ADNI-2 contains 150 ND, 150 SMC, 150 MCI and 150 AD. The ADNI-3 contains 133 ND, 151 MCI, 87 AD. The Australian imaging Biomarker & Lifestyle Flagship Study of Aging (AIBL) (AIBL, n.d.) database contains more than 1000 participants. The dataset contains the images of AD, MCI and CN. Open Access Serious of Imaging Studies (OASIS) dataset (OASIS, n.d.) collected from nearly 1000 participants. It contains 609 CN, 489 MCI patients MRI images. The collected MRI images are utilized for the analysis and detection of stages of AD.

TABLE 2 Overall images

Samples (MRI images)	Classes/Stages of AD			
	CN	SMC	MCI	AD
Train size	2560	1792	717	52
Test size	640	448	179	12

3.2 | Resizing

The input MRI images have been resized to reduce memory usage and increase classification performance. All the input image sizes are normalized during the resizing process as $240 \times 256 \times 176$ voxels images are, after pre-processing, resized as $96 \times 96 \times 64$, the resizing range [96 96 64]. The rescaled image quality needs to enhance for better prediction. The normalization range of the input image is rescaled [0, 1]. The minimum range for normalization is 0, and the maximum range is 1. This process facilitates the reduction of the memory utilization of the stages AD detection system.

3.3 | Adaptive filtering

Noise removal is an essential step in preprocessing to preserve the MRI images' biomarkers (edge of brain neuron); it helps predict performance. The Gaussian (white) noise in an MRI image reduces prediction accuracy. The adaptive filtering approach produces better filtering results than linear filtering. For better classification and memory usage, input MRI images were resized. It is possible to resize all of your images to the same size using the pre-processing step, which normalizes the dimensions of all of your images. For more accurate forecasting, the image quality after rescaling must be improved. [0, 1] is the new normalization range for the input image. It preserves edges and other high-frequency parts of an MRI image. The mathematical derivation of the adaptive filtering is as follows,

$$\hat{f}(a,b,c) = g(x,y) - \left(\frac{\sigma_h^2}{\sigma_L^2} \right) [g(a,b,c) - m_L] \quad (1)$$

where in Equation (1) the σ_h^2 denotes the overall noise, σ_L^2 denotes local variance of the local region, m_L denotes local means and $g(a,b,c)$ denotes the noisy image's voxel values at the position (a,b,c) . The notations s_h^2, s_L^2 indicates noise variance and local variance of the specific region s_{xy} , respectively. The following three conditions facilitate to filter noise and preserve biomarkers edges.

Condition 1. if $(s_h^2 = 0)$, return simply the value of $g(x,y)$.

Condition 2. $(s_L^2 > s_h^2)$, return a value close to $g(x,y)$ (high local variance associated with edges are preserved).

Condition 3. if $(s_L^2 = s_h^2)$, return arithmetic mean m_L .

- Simplifying the value
- A value close to high variance
- Arithmetic mean value

The noises in MRI imaging is a common issue, and it has been filtered by using the Equation (1) based on the above three conditions to preserve biomarkers edges. The next essential stage of the convolution layer is image enhancement.

3.4 | Adaptive histogram equalization

The sliding window adaptive histogram equalization approaches have been utilized in the framework for image enhancement. Unlike other equalization approaches, it creates several histograms; each corresponds to a distinct section of the MRI images and uses them to redistribute the lightness value of the MRI. Therefore, it is suitable for local contrast and enhances the edge in the brain MRI image slices. Tiling the image is to slide

the rectangle one voxel at a time and only additionally update the histogram for voxel by adding a new voxel row and subtracting the row left behind. The histogram calculation's computational complexity condenses from $O(N^2)$ to $O(N)$. N indicates the width of the surrounding rectangle. Adaptive histogram equalization improves by transforming each voxel with a transformation function derived from the neighbourhood region. It can also simplify as each voxel is transformed based on the square's histogram surrounding it. The resultant enhanced MRI image has been taken as input for filtering the noise. In picture improvement, sliding window adaptive histogram equalization algorithms have been used. While previous equalization methods employ a single histogram to spread the MRI brightness value throughout the image, this method uses many histograms that correlate to a different portion of the image. Local contrast and sharpening of the brain slices can be achieved by using this filter.

According to the results of the performance evolution, the new adaptive filter outperforms other comparison filtering approaches and is therefore suitable for biomedical image reconstruction. Extensive ultrasound scans were used to demonstrate the efficacy of a new framework for robust contrast enhancement and multiplicative noise suppression.

Figure 2a,b, left corner MRI brain images and right side normalized histogram of both the image samples. The AHE approach utilization facilitates enhancing image quality.

3.5 | Voxel-based morphometry (VBM)

The adaptive histogram equalization based enhanced images has been utilized for ROI region segmentation. The VBM approach segment the ROI of an image based on three voxel classes: white matter (WM), grey matter (GM), and cerebrospinal fluid (CF). The significant value of the grey matter cluster is $\rho < 0.05$ correction. The local maxima of the various biomarker regions and voxel values are right cerebellum (20, -62, -64), entorhinal area (27, 0, -20), amygdalae (-24, -2, -18), right posterior insula (38, -6, -2), right inferior temporal gyrus (57, -63, -15), and the right inferior occipital gyrus (44, -78, -12). The biomarker regions are segmented using grey matter the significant value (ρ) from the local maxima of the biomarker mentioned above regions.

Figure 3 illustrates the sample pre-processed and VBM based segmented MRI brain images of four stages of AD. The MCI, AD, CN, and SMC stages are displayed in the first, second, third, and fourth rows. The segmented biomarkers region's features are taken for feature extraction. The MRI biomarker characteristics of the brain's segmented biomarker regions are extracted using various feature extraction methods. This study used GLCM, Gabor, and wavelet features to extract the MRI image's biomarker information from the grey level.

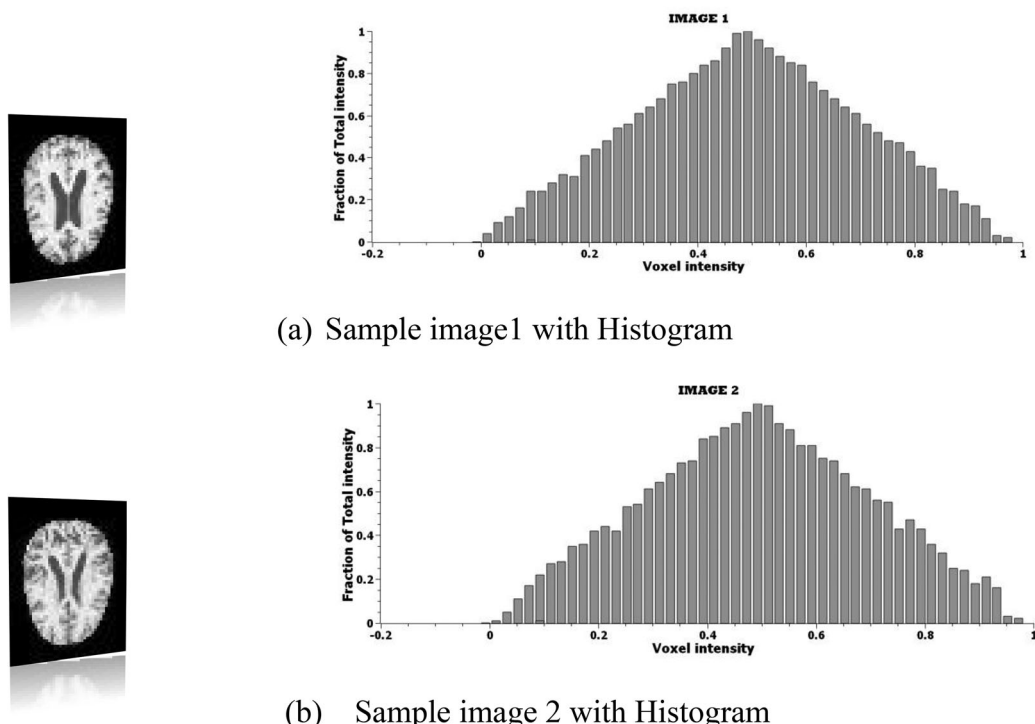


FIGURE 2 Sample adaptive histogram equalization (AHE) results. (a) Sample image 1 with histogram. (b) Sample image 2 with histogram

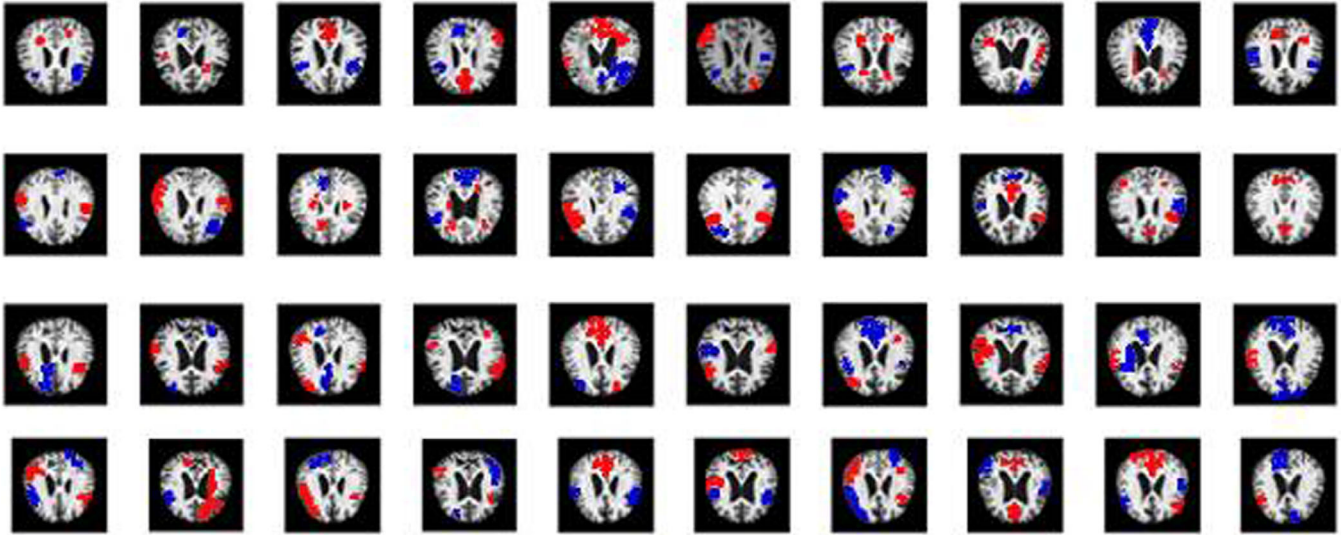


FIGURE 3 Segmented sample biomarkers of CN, SMC, MCI, and AD regions

3.6 | Feature extraction

Different feature extraction methods are applied to extract the brain's segmented biomarker regions' MRI biomarker features. This research applied grey-level co-occurrence matrices (GLCM), Gabor, and wavelet features to extract the MRI image's biomarker information. GLCM feature extracts the numerical features using spatial relationships of similar grey tones.

$$\text{Contr} = \sum_{r=1}^{\text{Ngl}} \sum_{c=1}^{\text{Ngl}} |r-c|^2 \text{GM}(r,c) \quad (2)$$

where in Equation (2) symbol Ngl denotes the number of discrete grey level and r represents the row, and c represents column and $\text{GM}(r,c)$ – grey level co-occurrence metrics. It is used to extract the contrast feature value of the M image.

$$\text{Corrm} = \frac{\sum_{r=1}^{\text{Ngl}} \sum_{c=1}^{\text{Ngl}} (rc) \text{GM}(r,c) - \mu_x(r) \mu_y(c)}{\sigma_x(r) \sigma_y(c)} \quad (3)$$

where in Equation (3) symbol $\mu_x(r)$ and $\mu_y(c)$ denotes the mean of row and column, $\sigma_x(r)$ and $\sigma_y(c)$ denotes the standard deviation of the row and column, which is used to extract the correlation feature value of the MRI image.

$$\text{Entr} = - \sum_r \sum_c \text{GM}[r,c] \ln(\text{GM}[r,c]) \quad (4)$$

The Equation (4) is used to estimate the entropy value of an MRI image. The $\text{GM}[r,c]$ is the grey tone spatial dependence matrix, and the r , c denotes row and columns values, and Ngl is the number of dissimilar grey levels in the quantized image.

$$\text{ClustPro} = \sum_{r=1}^{\text{Ngl}} \sum_{c=1}^{\text{Ngl}} [r+c - \mu_x(r) - \mu_y(c)]^4 \text{GM}(r,c) \quad (5)$$

$$\text{ClustShade} = \sum_{r=1}^{\text{Ngl}} \sum_{c=1}^{\text{Ngl}} [r+c - \mu_x(r) - \mu_y(c)]^3 \text{GM}(r,c) \quad (6)$$

$$\text{ClustTen} = \sum_{r=1}^{\text{Ngl}} \sum_{c=1}^{\text{Ngl}} [r+c - \mu_x(r) - \mu_y(c)]^2 \text{GM}(r,c) \quad (7)$$

where the Equation (5), Equation (6) and Equation (7) are used to calculate the cluster prominence, cluster shade and cluster tendency values of the segmented biomarker regions. The notation μ_x denotes mean of row and μ_y denotes the mean of the column. The GLCM based statistical relationships of various texture feature information of the biomarker textures are extracted to train the model.

3.7 | Gabor filter feature

The mathematic derivation of Gabor filter-based feature extraction has been represented as follows,

$$\text{Enr}_k = \frac{1}{rc} \sum_{x=0}^{r-1} \sum_{y=0}^{c-1} |I_f(x,y)|^k \quad (8)$$

where the Equation (8) is the classical method for extraction of Gabor filter based texture feature is the energy Enr_k , $k = 1, 2$ in the form of l_1 -norm and l_2 -norm. The notation r and c are the sizes of the sub-band intensity $I_f(x,y)$. The Gabor energy-based texture features information of the biomarker textures extracted to train the model.

The 3 Tesla T1 weighted MRI scanner is typically used to gather the input picture. For the purposes of this study, the 3D MRI baseline pictures were obtained using 3 Tesla T1 weighted images from the Alzheimer's Disease Neuroimaging Initiative (ADNI) database. 1.5 T or 3 T scanners are used to acquire structural T1 weighted MRI scans.

3.8 | Wavelet

The fundamental idea of DWT is to deliver time-frequency depiction. The 2D-DWT signifies an image in terms of a set of shifted and dilated wavelet functions $\omega^{\text{LH}}, \omega^{\text{HL}}, \omega^{\text{HH}}$ and scaling functions ϕ that form an orthonormal basis for $L^2(\mathbb{R}^2)$. Given a J -scale DWT, an image $x(r,c)$ of $M \times M$ is decomposed as follows,

$$x(r,c) = \sum_{p,o=0}^{N,q-1} u_{p,q,o} \phi_{p,q,o}(r,c) + \sum_{B \in B} \sum_{j=1} \sum_{q,o=0}^{M-1} w_{p,q,o}^B \omega_{p,q,o}^B(r,c) \quad (9)$$

with

$$\begin{aligned} \phi_{p,q,o}(r,c) &= 2^{-\frac{p}{2}} \phi(2^{-p}s - q, 2^{-p}t - o), \omega_{p,q,o}^B(r,c), \omega_{p,q,o}^B(r,c) \\ &2^{-\frac{p}{2}} \omega^B(2^{-p}s - q, 2^{-p}t - o), B \in B, B \end{aligned} \quad (10)$$

where the value of M is denoted as $M_p = M/2^p$ and the Equation (9) is used for the decomposition of the image $x(r,c)$ and Equation (10) represents the derivative of the scaling function. In this research, the LH, HL, and HH are named wavelet or DWT sub-band. $u_{p,q,o} = \int \int x(r,c) \phi_{p,q,o} ds dt$ is a scaling coefficient and $w_{p,q,o}^B = \int \int x(r,c) \omega_{p,q,o}^B ds dt$ denotes the $(q,o)^{\text{th}}$ wavelet coefficient in scale p and sub-band B . The derivation of wavelets in Equation (9) and Equation (10) facilitates extracting the wavelet feature information to train the model. The above-discussed features extraction techniques are utilized in this research to extract the biomarkers feature information from MRI images. The MRI biomarker features of the brain's segmented biomarker regions are extracted using various feature extraction methods. This study extracted the MRI image biomarker information using GLCM, Ga-bor, and wavelet features. The GLCM feature uses spatial relationships between grey tones that are similar in tone to get the numerical features.

3.9 | Hilbert Schmidt independence criteria lasso HSICL based feature selection

The HSICL approach performs well on both high and low dimensional samples. Therefore, the framework has been utilized the HSICL method to reduce more irrelevant features or significant features among extracted MRI biomarker features. The HSICL optimization has been given as follows,

$$\text{HSICL} : \min_a \frac{1}{2} \sum_{NN,m=1}^o a_{NN} a_m \text{HSIC}(f_{NN}, f_m) - \sum_{NN=1}^o a_{NN} \text{HSIC}(f_{NN}, c) + \lambda \|a\|_1, a_1, \dots, a_n > 0, \quad (11)$$

The Equation (11) is also written as follows,

$$\text{HSICL} : \min_a \frac{1}{2} \left\| \hat{L} - \sum_{NN=1}^o a_{NN} \hat{K}^{(NN)} \right\|_F^2 + \lambda \|a\|_1, a_1, \dots, a_o > 0 \quad (12)$$

The Equation (12) is used to reduce significant features from the various extracted MRI biomarkers features. Where $HSIC(f_{NN}, c) = \text{tr}(K^{(NN)} \hat{L})$ is a kernel-based independence measure called the empirical HSIC, $\text{tr}(\cdot)$ denotes the trace, λ is the regularization parameter, $K^{(NN)} = \Gamma K^{(NN)} \Gamma$ and $\hat{L} = \Gamma L \Gamma$ are input and output centred Gram matrices of MRI biomarkers features. $K_{ij}^{(NN)} = K(u_{NNi}, u_{NNj})$ and $L_{ij} = L(c_i, c_j)$ are Gram matrices, $K(u, u')$ and $L(c, c')$ are the two kernel functions. $\Gamma = I_o - \frac{1}{o} \mathbf{1}_o \mathbf{1}_o^T$ is the centring matrix, I_o is the o -dimensional identity matrix (number of biomarker features). $\mathbf{1}_o$ is the o dimensional vector with all ones, and $\|\cdot\|_1$ is l_1 -norm. The HSIC approach in the AD detection system helps identify the minimal set of biomarkers features to train the models, which helps avoid the over-fitting issue in the earlier detection system.

3.10 | FSODSNN based classifier

3.10.1 | Triple ranking loss

Traditionally, a CNN model trains to predict multiple AD classes. This creates confusion when a new class of AD stages needs to add or removed from the dataset, so the network model needs to retrain again. However, the DSNN learns based on similarity function; therefore, it can see if the two images are identical. This network feature helps to classify new classes of data without training again. The DSNN architecture contains the same configurations with the same parameters and weighted sub-networks, as well as the parameter updating process has been parallelized across both sub-networks. Therefore, the edge of the brain MRI image slices is enhanced, making it ideal for local contrast. One way to tile an image is to slide it around voxel-by-voxel, only updating the histogram for each voxel by adding new rows and taking away the old ones. Histogram computations are reduced from $O(N^2)$ to $O(N)$.

The learning in the DSNN can be done with triple loss or constructive loss. In this research, the Triple loss function is taken to compute the loss value. The selected features from the biomarker feature vectors are taken as input to train the DSNN model. During the model training, the DSNN model uses the triple ranking loss function to calculate loss, where a Training Sample image/input (TS) of AD is compared with Actual Positive image/input (AP) and Actual Negative/false image/input (AN). The calculated distance between the training sample and positive sample must be minimized, and the distance between the training sample and negative sample must be maximized. The loss value is calculated using the Triple Loss Function in this study. In training the DSNN model, the biomarker feature vectors are used as input. The DSNN model uses the triple ranking loss function to calculate loss during model training. The mathematical derivative of triple loss is represented as follows,

$$L(TS, AP, AN) = \max(\|f(TS) - f(AP)\|^2 - \|f(TS) - f(AN)\|^2 + m, 0) \quad (13)$$

It is imperative to reduce the distance estimated between the training and the positive samples and maximize this distance between the training and the negative samples. The triple-loss derivative's calculus is depicted here. Equation (13) is used to calculate the Loss value during the model train process. m denotes the maximum distance threshold. The function $f(TS/AP/AN)$ is used to compute the representation for three triplet elements. The maximum and minimum distance-based loss calculating feature of the triplet loss function helps predict loss during the backpropagation. It is used to discover the similarity among stages (MCI/AD/CN/SMC) by comparing feature vectors. Relu activation function performs well with DSNN models, so ReLU is taken for state activation function during the model training.

3.11 | Relu-activation function

ReLU is less computational complex than sigmoid and tangent activation function and helps avoid vanishing gradient problems. Therefore, ReLU is utilized for the state activation function in the DSNN model. The Rectified Linear Unit ReLU function $\max(0, z)$ and derivative $ReLU'$ is denoted as follows,

$$ReLU(z) = \begin{cases} z & z > 0 \\ 0 & z \leq 0 \end{cases} \quad \forall z = -1, \dots, 1 \quad (14)$$

Comparing feature vectors can be used to determine whether two stages (MCI/AD/CN/SMC) are alike. A state activation function that works well with DSNN models, like ReLU, has been used in the model training process in Equation (14).

$$ReLU'(z) = \begin{cases} 1 & z > 0 \\ 0 & z < 0 \end{cases} \quad \forall z = -1, \dots, 1 \quad (15)$$

The state activation conditions of ReLu has been given in Equation (15) and Equation (15). During the model training, each node's prediction loss and hyperparameters values have ReLu have handled the framework's state activation functionalities. The relu function activates the state when the parameter value is between -1 to 1 .

3.12 | Optimizer

The fish swarm optimizer has been incorporated in the DSNN model to identify new MRI (AD class) samples. It helps update the DSNN model's network nodes' parameters weight during the model training and prediction. The multi-objective behaviour of the fish swarm has been utilized for weight optimization, such as Target behaviour, Random behaviour, Teeming behaviour, Following based convergence, and Random behaviour, to optimize the network nodes parameters weight during the hyperparameter values updating process. The position of the input is represented as 3DMRI image feature vector (attribute) A ,

$$A = (a_{m1}, a_{m2}, \dots, a_{mn}) \quad (16)$$

In Equation (16), the DSNN model's convolution layers contract the input feature vector A . The fitness function of the target (B) is denoted as A_m .

$$d_{mn} = \|a_n - a_m\| \quad (17)$$

Hence, in Equation (17), the derivation of d_{mn} is used to calculate the distance between n and m of the specific attribute.

The target searching behaviour contains two conditions, in the first condition if $f(B_n) = f(A_m)$ then, it is considered as convergence. So it takes value towards $A_m A_n$, otherwise randomly choose the next state A_n .

$$\vec{A}_m = \begin{cases} \text{if } f(B_n) < f(A_m), A_m + \text{step } a \frac{A_n - A_m}{d_{mn}} \\ \text{else, random search} \end{cases} \quad (18)$$

where \vec{A}_m denotes the new state of the input attribute and the random interval value $[0,1]$. The Equation (18) is used to calculate the target behaviour function based convergence.

This phase takes fitness value for centroid (cen) of the target attribute or neighbour attribute value Nei_{iatr} and the group factor of the target attribute. Checking if $f(B_{cen})/Nei_{iatr} < \partial a B_n$ It takes the centroid (cen) of attributes else, and it remains in the target position. Where ∂ represents group factor, the range values assigned as $\in (0,1)$. The mathematical notation of the teeming behaviour-based optimization is denoted as follows,

$$\vec{A}_m = \begin{cases} \text{if } f(B_{cen})/Nei_{iatr} < \partial a B_n, A_m + \text{step } a \frac{A_{cen} - A_m}{d_{m,cen}} \\ \text{else, targeting position} \end{cases} \quad (19)$$

Equation (19) is used to calculate the teeming behaviour-based function to convergence.

The phase computes local minima of a current neighbour of A_m based convergence approach. It checks if the target attributes local minima lm of current neighbours value is $\partial a B_m$ then takes towards local minima of current neighbour; otherwise, it chooses target behaviour value. The mathematical notation of the following behaviour-based optimization is denoted as follows,

$$\vec{A}_m = \begin{cases} \text{if } f(B_{lm})/Nei_{fish} < \partial a B_m, A_m + \text{step } a \frac{A_{lm} - A_m}{d_{m,lm}} \\ \text{else, targeting position} \end{cases} \quad (20)$$

where Equation (20) is used to calculate the following based convergence functions, the fish selects position by visual range; likewise, the input parameter of the DSNN classifier weight updating position value by choosing any one of the local minima of a neighbour as convergence value. Likewise, whenever the new biomarker pattern of AD stages arrives for training or testing, the special new direction-finding behaviours of the fish swarm optimizer in the DSNN classifier helps to predict the possible AD stages. In this research, the above-discussed image processing methodologies and their features are combined to create the FSODSNN model for classifying the T1 MRI brain image based on Alzheimer's disease.

The above Pseudocode 1 gives the overall functionalities of the FSODSNN based AD stages detection framework. The collective benefit of early discussed features of this detection system helps to detect AD stages better. The performance of the FSODSNN model has been discussed in the subsequent section.

PSEUDOCODE 1 FSODSNN based AD detection framework**Input:** 3D MRI brain image**Step 1: Image accusation**

```
A = imread(data source) // Acquire input images from dataset
h = 0, bi = U = 0.02; // initialize the population, hidden layer size, bias & learning rate
```

Step 2: Convolution functions

```
For each i = 1 to TSC // TSC - Total number of sample images
RA = imresize(A, [96 96 64]) // resizing the input image
RS = rescale(RA) // Normalize the image (range from 0 to 1)
EA = adapthisteq(RS) // Adaptive histogram equalization
AF = imadaptfilt(EA) // Adaptive filtering
ROI = Vbm(AF, p < 0.05) // voxel based morphometry segmentation
For each j = 1 to TNF // TNF - total number of features
gabor[i, j] = imgaborfilt(ROI) // Gabor feature value
wavelet[i, j] = wav_fea(ROI) // wavelet feature value
GLCM = GLCM_features1(ROI) // GLCM features
Contr[i, j] = contr(GLCM)
Corn[i, j] = corrn(GLCM)
entr[i, j] = entr(GLCM)
clustPro[i, j] = clusterPro(GLCM)
clustShad[i, j] = clustshad(GLCM)
clustTen[i, j] = clustTen(GLCM)
FV[Contr[i, j], corn[i, j], entr[i, j], gabor[i, j], clustPro[i, j], clustShad[i, j], clustTen[i, j],
wavelet[i, j]] // biomarker feature vector
End For
End For
Reduct_set = HSICL(FV) // feature selection
FV = Reduct_set
```

Step 3: Classification phase

```
For each t = 1 to m // (m, n) = 1to Size (FV)
For each h = 1 to n
 $\emptyset$  (W. FV[t] + U. h + bi) // compute Relu  $\emptyset$  value for state activation
If ( $\emptyset$  >  $\emptyset$ minus; 1) && ( $\emptyset$  < 1)
Loss = L(TS, AP, AN) // triplet loss
End If
If (Loss <=  $\emptyset$ )
 $O_t$  // display output (predicted stage of AD)
Else
 $\vec{A}_m$  (FV(t+1)) // update the network node weight by using FSO based back propagation
End If
End For
End For
End For
Output: Detect stage of AD
```

4 | RESULTS AND DISCUSSIONS

This section discusses the performance evolution of the new AD detection framework. The AD detection framework's excellence is determined with various evaluation metrics (Haq et al., 2018), such as accuracy, sensitivity, specificity, error rate, Mathew's Correlation coefficient, and F-measure. The AD stages classification system has been implemented in the MATLAB simulator. The system performance has been compared with various existing deep classifiers such as traditional CNN, DSNN, ResNet, and VGG16. This comparison classifiers contribution to AD detection

has been discussed earlier in a related study. The numerical data provided in the research paper for the new AD detection framework's performance evolution is discussed in this section. Various evaluation metrics are used to gauge the effectiveness of the AD detection framework.

$$\text{Accuracy (Acc)} = \frac{\alpha + \beta}{\alpha + \beta + \delta + \gamma} \quad (21)$$

$$\text{Matthews's correlation coefficient (MCC)} = \frac{\alpha \cdot \beta - \gamma \cdot \delta}{\sqrt{(\alpha + \gamma)(\alpha + \delta)(\beta + \gamma)(\beta + \delta)}} \quad (22)$$

$$\text{Recall} \vee \text{Sensitivity (Sen)} = \frac{\alpha}{\alpha + \delta} \quad (23)$$

$$\text{Specificity (Speci)} = \frac{\beta}{\beta + \gamma} \quad (24)$$

$$F\text{-measure}(F_{\text{measure}}) = \frac{(1 + \beta^2)(\text{Speci} \cdot \text{Sen})}{(\beta^2 \cdot \text{Speci} + \text{Sen})} \beta = 0.5, 1, \vee 2 \quad (25)$$

$$\text{Errorrate (Errat)} = \frac{\gamma + \delta}{\text{Positive} + \text{Negative}} \quad (26)$$

The notations $\alpha, \beta, \gamma \wedge \delta$ in Equation (21), Equation (22), Equation (23), Equation (24), Equation (25) and Equation (26) denotes the true negative and true positive, false negative and false positive, respectively. These metrics are utilized in this research to assess the performance of the AD detection system.

Table 3 shows the consolidated performance comparison of the convolution-based **FSODSNN** framework with CNN, ResNet, VGG16 and DSNN for AD stages detection. It clearly shows that the new classification framework's highest accuracy rate (99.89%) is achieved by using the specific features of the new convolution layers functionalities in FSODSNN such as resizing, filtering, biomarker region preserving or enhancement, biomarkers regions based feature segmentation, extraction and reduction are performing efficiently during the pre-processing phase.

Figure 4 illustrates that the new food source direction investigation features of FSO in the DSNN network help efficiently optimize the image features training functionalities. The new food source direction investigation of FSO is derived as,

$$\vec{A}_m = \begin{cases} \text{if } f(B_{lm}) / \text{Nei}_{\text{fish}} < \partial a B_m, A_m + \text{step } a \frac{A_{lm} - A_m}{d_{m,lm}} \\ \text{else, targeting position} \end{cases}$$

accuracy metrics.

TABLE 3 Overall performance of classifiers in AD detection comparison

Dataset	Classifier	Accuracy (%)	MCC (%)	Sensitivity (%)	Specificity (%)	F_{measure} (%)	Error rate (%)
ADNI	CNN	94.82	93.98	94.23	94.32	93.88	5.19
	ResNet	96.22	95.66	96.29	95.43	96.76	3.78
	VGG16	98.45	98.23	98.43	98.76	98.65	1.55
	DSNN	98.79	99.03	99.01	99.18	99.45	1.21
	FSODSNN	99.89	99.67	99.55	99.25	99.66	0.11
AIBL	CNN	94.81	93.75	94.76	94.45	93.45	5.21
	ResNet	96.22	95.34	96.43	96.65	96.87	3.56
	VGG16	98.45	98.45	98.87	98.74	98.98	1.73
	DSNN	98.88	98.99	98.54	98.98	99.87	1.12
	FSODSNN	99.67	99.86	98.81	99.28	99.45	0.14
OASIS	CNN	94.86	93.65	94.65	94.99	93.45	5.14
	ResNet	96.43	95.45	96.73	95.66	96.45	3.57
	VGG16	98.74	97.56	98.97	97.89	98.76	1.26
	DSNN	98.87	99.54	99.51	98.77	99.12	1.13
	FSODSNN	99.61	99.76	99.62	99.11	99.22	0.35

Note: The values in bold letter denotes the maximum value for each metric that has been obtained by the new classification (**FSODSNN**) approach.

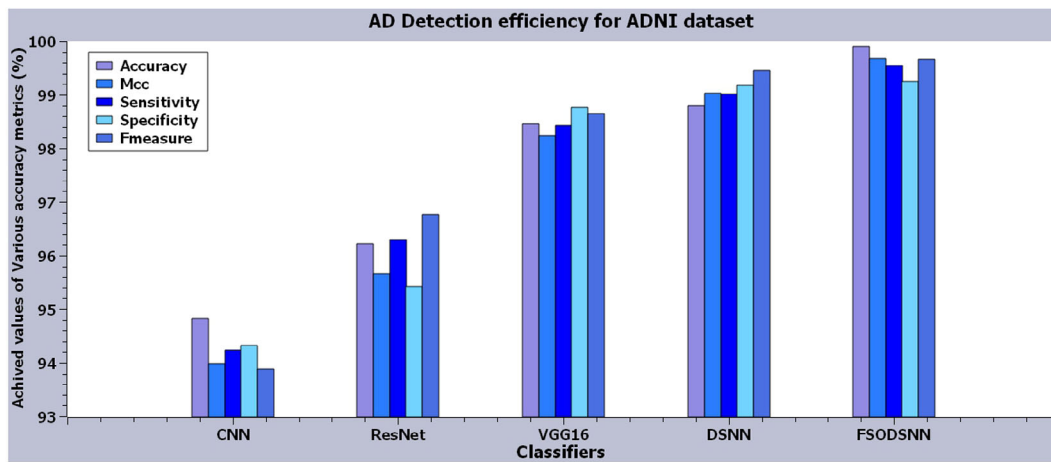


FIGURE 4 Performance comparison of FSODSNN with other classifiers using ADNI dataset

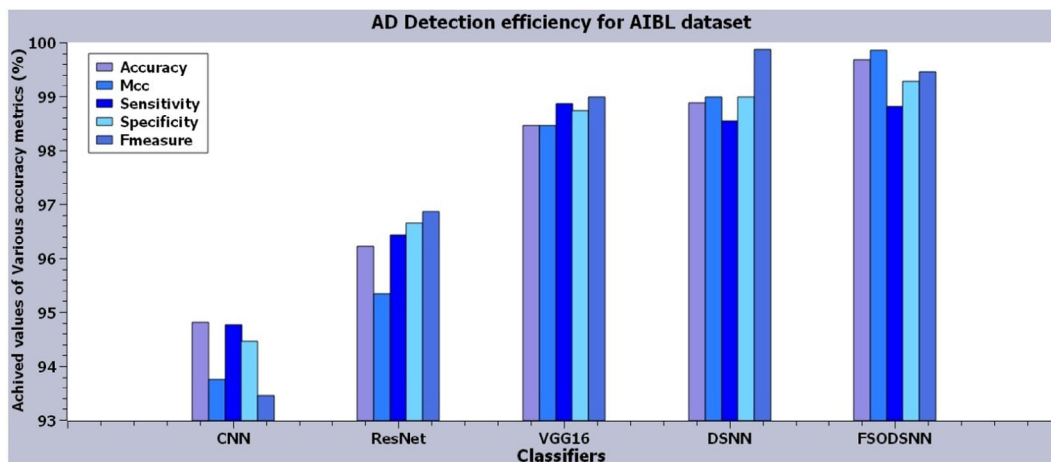


FIGURE 5 Performance comparison of all the classifiers using AIBL dataset

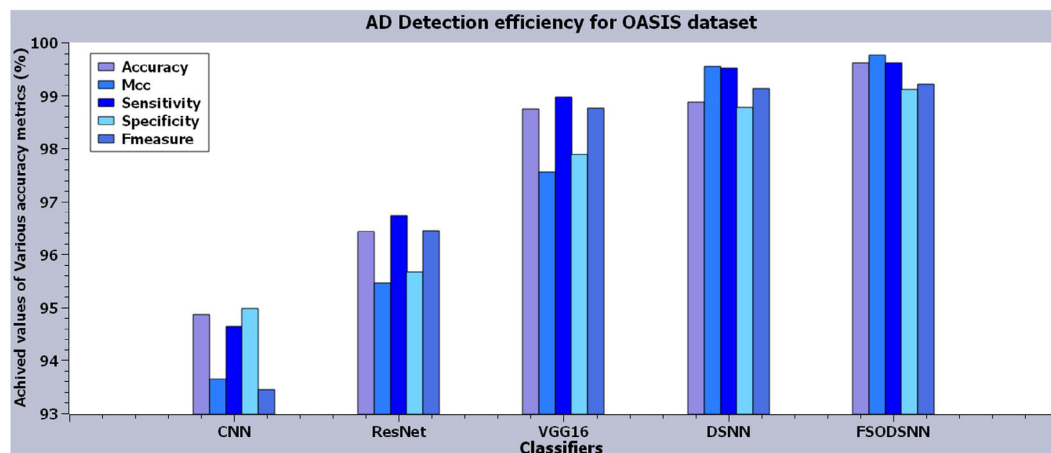


FIGURE 6 Performance comparison of all the classifiers using OASIS dataset

Figure 5 illustrates the graphical representation of the efficiency evaluation results for the AIBL dataset. The FSODSNN based AD stages detection approach has outperformed all the accuracy metrics. It is clear proof that the new methodologies based on convolution layers functionalities help identify and extract biomarkers regions proficiently during the model training in FSODSNN classifiers for AD stages detection framework more efficiently than other classifiers.

Figure 6 illustrates that the FSODSNN based AD stages detection approach outperforms accuracy. It clearly shows that the incorporated functionalities of convolution layers (adaptive filtering, adaptive histogram equalization based image enhancement, VBM based grey matter cluster ($\rho < 0.05$) of biomarker region segmentation and extraction). The FSODSNN model helps detect the AD stages more efficiently than other classifiers.

Figure 7 illustrates that the new convolution functionalities incorporated in FSODSNN based AD stages detection approach has been obtained, promising a lesser error rate (0.11%). The minimal error rate is achieved with the help of uncertainty reduction using DSNN's triplet loss function, which is derived in the following derivation, $L(TS, AP, AN) = \max(\|f(TS) - f(AP)\|^2 - \|f(TS) - f(AN)\|^2 + m, 0)$.

In Figure 8, the five different coloured curves show the graphical representation of accuracy rate comparison of CNN, ResNet, VGG16, DSNN and FSODSNN based AD stages detection with ADNI, AIBI and OASIS datasets. Moreover, the top three blue coloured curves denote the maximum accuracy rates of 99.89%, 99.67% and 99.61% for three datasets. The maximum accuracy is achieved by the FSODSNN model with the help of overfitting reduction (HSICL based feature reduction) function, which is derived in the following derivation, $HSICL: \min_a \frac{1}{2} \left\| \hat{L} - \sum_{NN=1}^o a_{NN} \hat{K}^{(NN)} \right\|_F^2 + \lambda \|a\|_1, a_1, \dots, a_o > 0$.

In Figure 9, the five different coloured curves show the graphical representation of Mathew's correlation coefficient values comparison of CNN, ResNet, VGG16, DSNN and FSODSNN based AD stages detection with ADNI AIBI and OASIS datasets. Moreover, each convolution layer's problem-oriented functionalities in the FSODSNN framework and the new food source direction investigation features of FSO in the DSNN

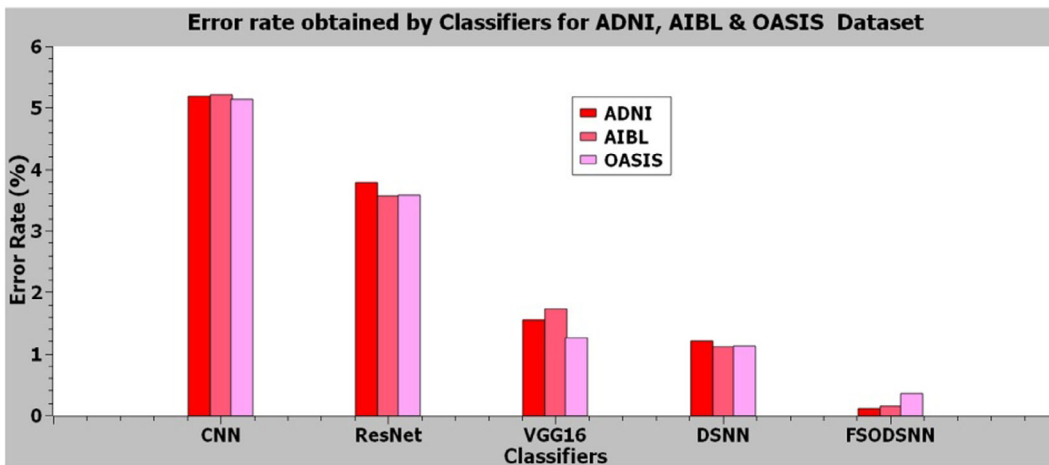


FIGURE 7 Error rate comparison for ADNI, AIBI and OASIS datasets

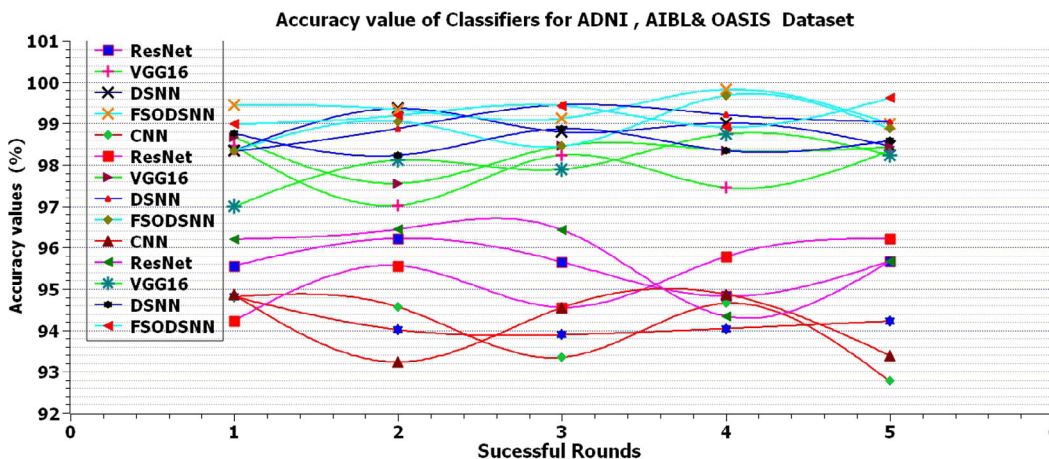


FIGURE 8 Accuracy rate comparison curves for ADNI, AIBI and OASIS datasets

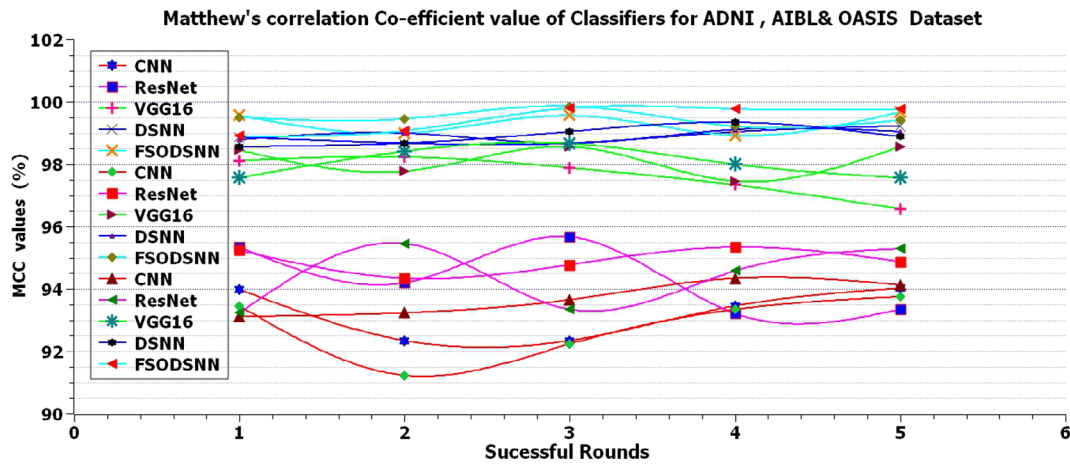


FIGURE 9 Mathew's correlation coefficient values comparison curves for ADNI, AIBI and OASIS datasets

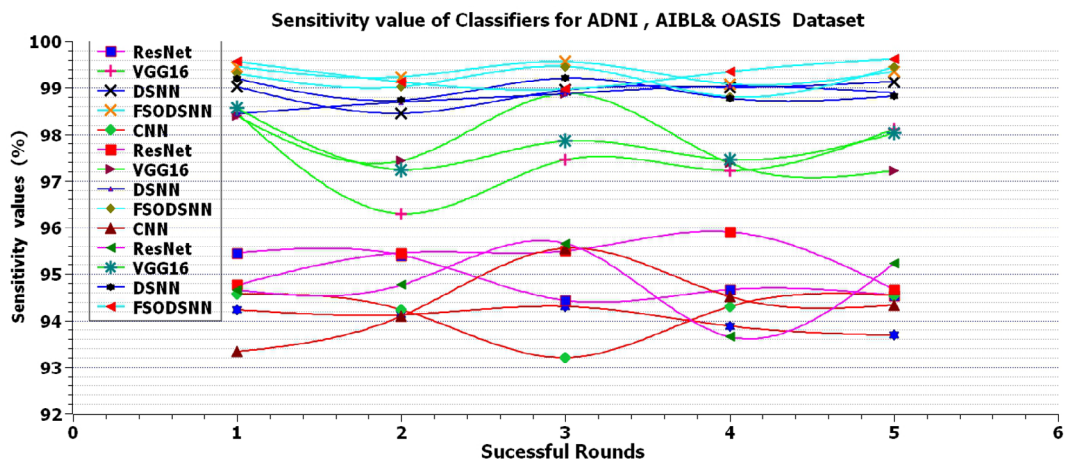


FIGURE 10 Sensitivity values comparison curves for ADNI, AIBI and OASIS datasets

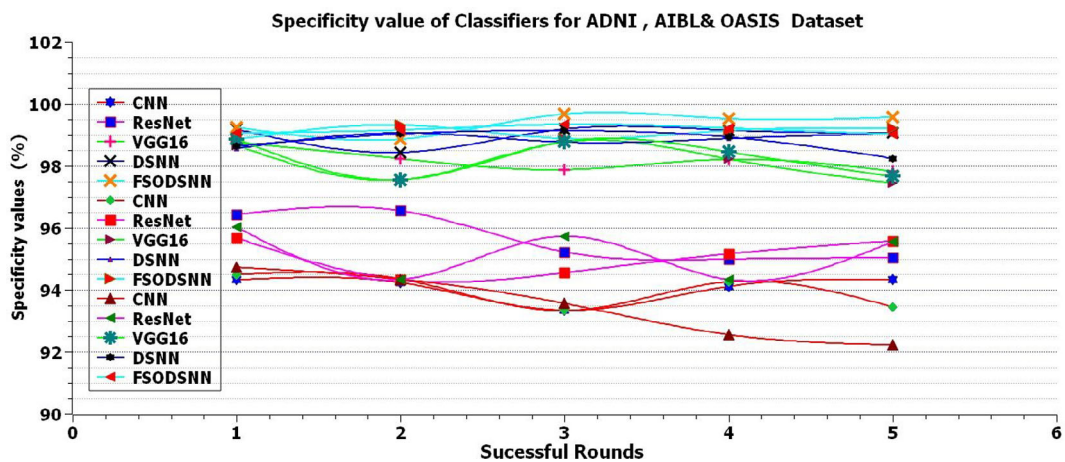


FIGURE 11 Specificity values comparison curves for ADNI, AIBI and OASIS datasets

network facilitate optimisation of the uncertainty issues efficiently. These two specific functions influence the classifier's performance to achieve maximum Mathew's Correlation coefficient values (99.67%, 99.86% and 99.81%) in five successful rounds for three different dataset images.

In Figure 10, the five different coloured curves show the graphical representation of Sensitivity values comparison of CNN, ResNet, VGG16, DSNN and FSODSNN based AD stages detection with ADNI, AIBI and OASIS datasets. Moreover, the top three blue coloured cures denote the

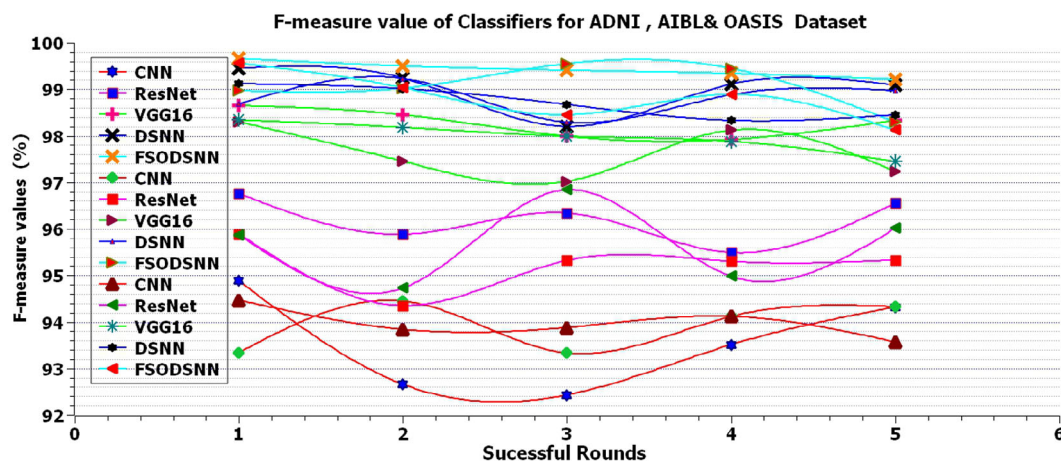


FIGURE 12 F-measures values comparison curves for ADNI, AIBI and OASIS datasets

VBM based grey matter segmentation ($p < 0.05$) of biomarker region and biomarkers, texture features extraction techniques to train the AD stages exactly. Therefore, these two convolution layer features play an essential role in achieving the maximum sensitivity (99.56%, 99.45% and 99.62%) compared to comparison approaches.

In Figure 11, the five different coloured curves show the graphical representation of Specificity values comparison of CNN, ResNet, VGG16, DSNN and FSODSNN based AD stages detection using ADNI, AIBI and OASIS datasets. Moreover, the uncertainty and overfitting reduction incorporated the FSODSNN approach influencing the classifier to acquire higher specificity values (99.67%, 99.14% and 99.34%) in AD stages detections.

In Figure 12, the five different coloured curves show that the new convolution functionalities incorporated FSODSNN model has been attained maximum F-measures values of 99.66%, 99.55% and 99.56% for ADNI AIBI and OASIS datasets, respectively.

The specific problem-oriented functionalities of each convolution layer in the FSODSNN framework and the new food source direction investigation features of FSO in the DSNN network facilitate to optimization of the uncertainty issues efficiently. These two features help achieve a maximum of 99.89% accuracy rate in AD stages detection. The DSNN's triplet loss function and HSICL based irrelevant feature reduction function reduce the overfitting issues. Overfitting reduces the classification framework to achieve the lowest error rate of 0.11% in AD stages detection other four convolutions based on comparison classification approaches. The section's overall evaluation outcome shows that the AD detection framework features, such as feature enhancement, exact biomarker region identification, and irrelevant feature information reduction, help reduce overfitting during model training. Furthermore, an uncertain biomarker feature classification issue has been resolved efficiently with FSO's functionalities in DSNN.

5 | CONCLUSIONS

Hence, the evaluation report in the results and discussion section shows that the new convolution-based AD detection framework has outperformed all the evolution metrics compared to comparison approaches. It clearly shows that the new sample training feature of FSO in DSNN helps resolve the uncertainty issues during the AD stages detection. The HSICL based feature reduction technique reduces unwanted feature information during the model training, reducing over-fitting problems. So in AD stages, the detection framework predicts the stages with less error than comparison algorithms. The suitable biomarker feature enhancement and biomarker region identification utilization helps to efficiently train the classification model, which has improved accuracy and error reduction. This research's main objective is to resolve the uncertainty, overfitting, biomarker region preserving and extraction issues. The overall evaluation result shows that the new AD detection model has been achieved the objective of the research reliably. In this research, the AD stages detection has been attained a maximum of 99.89% accuracy rate and 0.11% error rate.

The current research achieves the highest accuracy rate in the AD stages detection system; therefore, future research is trying to utilize the heuristic approach based on pixel examination to detect AD stages with maximum forecast rate.

The primary goal of this research is to address the challenges of uncertainty, overfitting, biomarker preservation, and extraction. Overall, the results suggest that the novel AD detection model met the study's accuracy goal. Currently, researchers are working to improve AD stage detection systems, and future study is looking to use the heuristic approach based on pixel examination to detect AD stages with the greatest forecast rate.

DATA AVAILABILITY STATEMENT

Data sharing is not applicable to this article as no new data were created or analyzed in this study.

ORCID

Rajaram Sampath  <https://orcid.org/0000-0002-3553-4569>

Manickam Baskar  <https://orcid.org/0000-0003-4655-7667>

REFERENCES

- Acharya, U. R., Fernandes, S. L., WeiKoh, J. E., Ciaccio, E. J., Fabell, M. K. M., Tanik, U. J., Rajinikanth, V., & Yeong, C. H. (2019). Automated detection of Alzheimer's disease using brain MRI images—A study with various feature extraction techniques. *Journal of Medical Systems*, 43, 302. <https://doi.org/10.1007/s10916-019-1428-9>
- Aderghal, K., Khvostikov, A., Krylov, A., Benois-Pineau, J., Afdel, K., & Catheline, G. (2018). Classification of Alzheimer disease on imaging modalities with deep CNNs using cross-modal transfer learning. In *Proceedings of the IEEE 31st International Symposium on Computer-Based Medical Systems (CBMS)* (pp. 345–350). IEEE.
- ADNI (n.d.). *Data source*. <http://adni.loni.usc.edu/data-samples/access-data/>.
- AIBL (n.d.). *Data source*. <https://aibl.csiro.au/adni/index.html>.
- Al-Kadi, O. S. (2017). A Gabor filter texture analysis approach for histopathological brain tumor subtype discrimination. *ISESCO Journal of Science and Technology*, 12(22).
- Allioui, H., Sadgal, M., & Elfazziki, A. (2020). Utilization of a convolutional method for Alzheimer disease diagnosis. *Machine Vision and Applications*, 31, 25. <https://doi.org/10.1007/s00138-020-01074-5>
- Beheshti, I., Demirel, H., & Matsuda, H. (2017). Classification of Alzheimer's disease and prediction of mild cognitive impairment-to-Alzheimer's conversion from structural magnetic resonance imaging using feature ranking and a genetic algorithm. *Computers in Biology and Medicine*, 83, 109–119. <https://doi.org/10.1016/j.combiomed.2017.02.011>
- Chen, Y., Jia, H., Huang, Z., & Xia, Y. (2018). Early identification of Alzheimer's disease using an ensemble of 3D convolutional neural networks and magnetic resonance imaging. In *Proceedings of the International Conference on Brain Inspired Cognitive Systems* (pp. 303–311). Cham: Springer.
- Cheng, D., & Liu, M. (2017). Classification of Alzheimer's disease by cascaded convolutional neural networks using PET images. In *Proceedings of the International Workshop on Machine Learning in Medical Imaging* (pp. 106–113). Springer International Publishing.
- Damodaran, B. B., Courty, N., & Lefèvre, S. (2017). Sparse Hilbert Schmidt independence criterion and surrogate-kernel-based feature selection for hyperspectral image classification. *IEEE Transactions on Geoscience and Remote Sensing*, 55(4), 2385–2398. <https://doi.org/10.1109/TGRS.2016.2642479>
- Dolph, C. V., Alam, M., Shboul, Z., Samad, M. D., & Iftekharuddin, K. M. (2017). Deep learning of texture and structural features for multiclass Alzheimer's disease classification. In *Proceedings of the International Joint Conference on Neural Networks (IJCNN)* (pp. 2259–2266). IEEE.
- Ebrahimi-Ghahnavieh, A., Luo, S., & Chiong, R. (2019). Transfer learning for Alzheimer's disease detection on MRI images. In *2019 IEEE International Conference on Industry 4.0, Artificial Intelligence, and Communications Technology (IAICT), BALI, Indonesia* (pp. 133–138). IEEE. <https://doi.org/10.1109/ICIAICT.2019.8784845>
- Ebrahimi-Ghahnavieh, M. A., Luo, S., & Chiong, R. (2020). Deep learning to detect Alzheimer's disease from neuroimaging: A systematic literature review. *Computer Methods and Programs in Biomedicine*, 187, 105242.
- Fan, Z., Xu, F., Qi, X., Li, C., & Yao, L. (2020). Classification of Alzheimer's disease based on brain MRI and machine learning. *Neural Computing and Applications*, 32, 1927–1936. <https://doi.org/10.1007/s00521-019-04495-0>
- Faturrahman, M., Wasito, I., Hanifah, N., & Mufidah, R. (2017). Structural MRI classification for Alzheimer's disease detection using deep belief network. In *Proceedings of the 11th International Conference on Information & Communication Technology and System (ICTS)* (pp. 37–42). IEEE.
- Garg, M., & Dhiman, G. (2020). A novel content-based image retrieval approach for classification using GLCM features and texture fused LBP variants. *Neural Computing and Applications*, 33, 1311–1328. <https://doi.org/10.1007/s00521-020-05017-z>
- Gupta, B., & Verma, A. R. (2020). A novel approach of 2D adaptive filter based on MPSO technique for biomedical image. *Augment Human Research*, 5, 1. <https://doi.org/10.1007/s41133-019-0017-2>
- Gupta, Y., Lee, K. H., Choi, K. Y., Lee, J. J., Kim, B. C., Kwon, G. R., National Research Center for Dementia, & Alzheimer's Disease Neuroimaging Initiative. (2019). Early diagnosis of Alzheimer's disease using combined features from voxel-based morphometry and cortical, subcortical, and hippocampus regions of MRI T1 brain images. *PLoS One*, 14(10), e0222446. <https://doi.org/10.1371/journal.pone.0222446>
- Haq, A. U., Li, J. P., Memon, M. H., Nazir, S., & Sun, R. (2018). A hybrid intelligent system framework for the prediction of heart disease using machine learning algorithms. *Mobile Information Systems*, 2018, 1–21. <https://doi.org/10.1155/2018/3860146>
- Hon, M. (2017). Towards Alzheimer's disease classification through transfer learning. In *2017 IEEE International Conference on Bioinformatics and Biomedicine (BIBM), Kansas City, MO* (pp. 1166–1169). IEEE. <https://doi.org/10.1109/BIBM.2017.8217822>
- Jha, D., & Kwon, G. (2017). Alzheimer's disease detection using sparse autoencoder, scale conjugate gradient and softmax output layer with fine-tuning. *International Journal of Machine Learning and Computing*, 7(1), 13–17.
- Ju, R., Hu, C., & Li, Q. (2019). Early diagnosis of Alzheimer's disease based on resting-state brain networks and deep learning. *IEEE/ACM Transactions on Computational Biology and Bioinformatics (TCBB)*, 16(1), 244–257.
- Karasawa, H., Liu, C.-L., & Ohwada, H. (2018). Deep 3D convolutional neural network architectures for Alzheimer's disease diagnosis. *Lecture Notes in Computer Science*, 10751, 287–296. https://doi.org/10.1007/978-3-319-75417-8_27
- Kazemi, Y., & Houghten, S. K. (2018). A deep learning pipeline to classify different stages of Alzheimer's disease from fMRI data. In *Proceedings of the IEEE Conference on Computational Intelligence in Bioinformatics and Computational Biology (CIBCB)* (pp. 1–8). IEEE.
- Kumari, R., Nigam, A., & Pushkar, S. (2020). Machine learning technique for early detection of Alzheimer's disease. *Microsystem Technologies*, 26, 3935–3944. <https://doi.org/10.1007/s00542-020-04888-5>
- Lee, G., Nho, K., Kang, B., Sohn, K.-A., & Kim, D. (2019). Predicting Alzheimer's disease progression using multi-modal deep learning approach. *Scientific Reports*, 9, 1952. <https://doi.org/10.1038/s41598-018-37769-z>

- Li, Y., Zhang, L., Bozoki, A., Zhu, D. C., Choi, J., & Maiti, T. (2020). Early prediction of Alzheimer's disease using longitudinal volumetric MRI data from ADNI. *Health Services and Outcomes Research Methodology*, 20, 13–39. <https://doi.org/10.1007/s10742-019-00206-3>
- Liu, C.-F., Padhy, S., Ramachandran, S., Wang, V. X., Efimov, A., Bernal, A., Shi, L., Vaillant, M., Ratnanather, J. T., Faria, A. V., Caffo, B., Albert, M., Miller, M. I., BIOCARD Research Team, & Alzheimer's Disease Neuroimaging Initiative. (2019). Using deep Siamese neural networks for detection of brain asymmetries associated with Alzheimer's disease and mild cognitive impairment. *Magnetic Resonance Imaging*, 64, 190–199.
- Liu, M., Li, F., Yan, H., Wang, K., Ma, Y., Shen, L., & Mingqing, X. (2020). A multi-model deep convolutional neural network for automatic hippocampus segmentation and classification in Alzheimer's disease. *NeuroImage*, 208, 1053–8119. <https://doi.org/10.1016/j.neuroimage.2019.116459>
- D. Lu, K. Popuri, G. W. Ding, R. Balachandar, M. F. Beg, and the Alzheimer's Disease Neuroimaging Initiative, "Multiscale deep neural network-based analysis of FDG-PET images for the early diagnosis of Alzheimer's disease," *Medical Image Analysis*, vol. 46, pp. 26–34, 2018.
- Lucas, F., Costa, P., Batalha, R., & Leite, D. F. (2020). Fault detection in smart grids with time-varying distributed generation using wavelet energy and evolving neural networks. *Evolving Systems*, 11, 165–180. <https://doi.org/10.1007/s12530-020-09328-3>
- Mori, S., Wu, D., Ceritoglu, C., Li, Y., Kolasny, A., Vaillant, M. A., Faria, A. V., Oishi, K., & Miller, M. I. (2016). MRICloud: Delivering high-throughput MRI neuroinformatics as cloud-based software as a service. *Computing in Science & Engineering*, 18(5), 21–35. <https://doi.org/10.1109/MCSE.2016.93>
- Nawaz, H., Maqsood, M., Afzal, S., Aadil, F., Mehmood, I., & Rho, S. (2020). A deep feature-based real-time system for Alzheimer disease stage detection. *Multimedia Tools and Applications*. 80, 35789–35807. <https://doi.org/10.1007/s11042-020-09087-y>
- OASIS (n.d.). *Data source*. <https://www.oasis-brains.org/>.
- Shi, B., Chen, Y., Zhang, P., Smith, C. D., Liu, J., & Alzheimer's Disease Neuroimaging Initiative. (2017). Nonlinear feature transformation and deep fusion for Alzheimer's disease staging analysis. *Pattern Recognition*, 63, 487–498.
- Singh, P., Mukundan, R., & De Ryke, R. (2020). Feature enhancement in medical ultrasound videos using contrast-limited adaptive histogram equalization. *Journal of Digital Imaging*, 33, 273–285. <https://doi.org/10.1007/s10278-019-00211-5>
- Solano-Rojas B., Villalón-Fonseca R., Marín-Raventós G. (2020) Alzheimer's disease early detection using a low cost three-dimensional Densenet-121 architecture. In: Jmaiel M., Mokhtari M., Abdulrazak B., Aloulou H., Kallel S. (eds) *The impact of digital technologies on public health in developed and developing countries*. ICOST 2020. *Lecture Notes in Computer Science* (vol 12157). Springer. https://doi.org/10.1007/978-3-030-51517-1_1
- Spalthoff, R., Gaser, C., & Nenadić, I. (2018). Altered gyrification in schizophrenia and its relation to other morphometric markers. *Schizophrenia Research*. 202, 195–202. <https://doi.org/10.1016/j.schres.2018.07.014>
- Spasov, S. E., Passamonti, L., Duggento, A., Lio, P., & Toschi, N. (2018). A multi-modal convolutional neural network framework for the prediction of Alzheimer's disease. In *2018 40th Annual International Conference of the IEEE Engineering in Medicine and Biology Society (EMBC)*. IEEE. <https://doi.org/10.1109/embc.2018.8512468>
- Ullah, H. M. T., Onik, Z., Islam, R., & Nandi, D. (2018). Alzheimer's disease and dementia detection from 3D brain MRI data using deep convolutional neural networks. In *2018 3rd International Conference for Convergence in Technology (I2CT), Pune* (pp. 1–3). IEEE. <https://doi.org/10.1109/I2CT.2018.8529808>
- Wang, S. H., Phillips, P., Sui, Y., Sui, Y., Liu, B., Yang, M., & Cheng, H. (2018). Classification of Alzheimer's disease based on eight-layer convolutional neural network with leaky rectified linear unit and max pooling. *Journal of Medical Systems*, 42, 85. <https://doi.org/10.1007/s10916-018-0932-7>
- Wee, C.-Y., Liu, C., Lee, A., Poh, J. S., Ji, H., & Qiu, A. (2019). Cortical graph neural network for AD and MCI diagnosis and transfer learning across populations. *NeuroImage: Clinical*, 23, 101929. <https://doi.org/10.1016/j.nicl.2019.101929>
- Ye, F., Shao, S., & Tian, Y. (2018). Weapon target assignment based on improved artificial fish swarm algorithm. In *2018 USNC-URSI Radio Science Meeting (Joint with AP-S Symposium), Boston, MA* (pp. 15–16). IEEE. <https://doi.org/10.1109/USNC-URSI.2018.8602636>

AUTHOR BIOGRAPHIES



Rajaram Sampath completed his undergraduate program in information technology from Madurai Kamaraj University. He completed his postgraduate program from SRM Institute of Science and Technology. At present he is a part time research scholar at SRM University Chennai. His area of interests includes Machine Learning, Deep Learning, image processing, artificial neural networks, Medical image processing and data mining. His research includes Alzheimer's disease prediction, body sensor networks, and disease prediction systems.



Manickam Baskar received B.E. Computer Science and Engineering from Anna University, Chennai, M.Tech. Information Technology from Sathyabama University, Chennai and Ph.D. (Information and Communication Engineering) from Anna University, Chennai. His Area of research interest includes Computer Networks and Security, Parallel and Distributed Systems, Image Processing, Big Data, Machine Learning, Deep Learning and IoT. He is published 7 Patents 54 Research Articles in reputed International Journals and 12 Article in International Conferences. He is acting as a reviewer in Cluster Computing, Journal of Web Engineering, Multimedia Tools and Applications, Neural Processing Letters, Concurrency and Computation: Practice and Experience, Journal of Ambient Intelligence and Humanized Computing and Computational Intelligence. He is a Life time Professional body member of CSI, ISTE, IET, ACM, ISRD, IRED, IACSET, IAENG, SDIWC and UACEE.

How to cite this article: Sampath, R., & Baskar, M. (2022). 3D brain image-based Alzheimer's disease detection techniques using fish swarm optimizer's deep convolution Siamese neural network. *Expert Systems*, e12963. <https://doi.org/10.1111/exsy.12963>